PHYSICAL REVIEW MATERIALS **1**, 071001(R) (2017)

First-principles engineering of charged defects for two-dimensional quantum technologies

Feng Wu,[1] Andrew Galatas,[2] Ravishankar Sundararaman,[3] Dario Rocca,[4,5] and Yuan Ping[1,*]

[1]*Department of Chemistry and Biochemistry, University of California, Santa Cruz, California 95064, USA*

[2]*Department of Physics, University of California, Santa Cruz, California 95064, USA*

[3]*Department of Materials Science and Engineering, Rensselaer Polytechnic Institute, 110 8th Street, Troy, New York 12180, USA*

[4]*Université de Lorraine, CRM2, UMR 7036, 54506 Vandoeuvre-lès-Nancy, France*

[5]*CNRS, CRM2, UMR 7036, 54506 Vandoeuvre-lès-Nancy, France*

(Received 25 September 2017; published 6 December 2017)

Charged defects in two-dimensional (2D) materials have emerging applications in quantum technologies such as quantum emitters and quantum computation. The advancement of these technologies requires a rational design of ideal defect centers, demanding reliable computation methods for the quantitatively accurate prediction of defect properties. We present an accurate, parameter-free, and efficient procedure to evaluate the quasiparticle defect states and thermodynamic charge transition levels of defects in 2D materials. Importantly, we solve critical issues that stem from the strongly anisotropic screening in 2D materials, that have so far precluded the accurate prediction of charge transition levels in these materials. Using this procedure, we investigate various defects in monolayer hexagonal boron nitride (*h*-BN) for their charge transition levels, stable spin states, and optical excitations. We identify C_BV_N (nitrogen vacancy adjacent to carbon substitution of boron) to be the most promising defect candidate for scalable quantum bit and emitter applications.

DOI: 10.1103/PhysRevMaterials.1.071001

Two-dimensional (2D) materials such as graphene, hexagonal boron nitride (*h*-BN), and transition-metal dichalcogenides exhibit a wide range of remarkable properties at atomic-scale layer thicknesses, holding promise for both conventional and new optoelectronic functionalities at drastically reduced dimensions [1–5]. It is well established that point defects play a central role in the properties of bulk three-dimensional (3D) semiconductors but their corresponding role in 2D materials is not yet well understood. In particular, the weak screening environment surrounding the defect charge distribution and the strong confinement of wave functions due to the atomic-scale thickness could lead to vastly different behaviors compared to conventional semiconductors.

Defects in 2D materials such as *h*-BN show promise as polarized and ultrabright single-photon emitters at room temperature [6,7], with potentially better scalability [8,9] than the long-studied nitrogen-vacancy center (NV) in diamond [10–12] for emerging applications in nanophotonics and quantum information [13]. Progress beyond the initial experimental demonstration of promising properties requires the rational design and development of quantum defects in 2D materials that exhibit a high emission rate, long coherence time, single photon purity, and stability. Specifically, the promising defects should have the following properties: Defect levels should be deep (far from the band edges) to avoid resonance with the bulk band edges and thereby exhibit a long coherence time [6,14,15]; optically addressable spin conserving excitations facilitate exploiting spin-selective decays in high-spin defect states, similar to the NV center in diamond [16–18]; anisotropic polarization of the defect states in combination with quantum bits could provide a pathway to quantum optical computation. A recent work [18] performed density functional theory (DFT) and constraint DFT calculations to obtain the Huang-Rhys factor and photoluminescence spectrum for multiple neutral defects in *h*-BN, while the possibility of forming charged defects has not been examined. Most importantly, a higher level of theory beyond DFT is necessary to obtain accurate defect charge transition levels, which has not been carried out for charged defects in 2D materials due to several technical difficulties that will be resolved here.

In this Rapid Communication, we use first-principles methods to theoretically investigate the suitability of several complex defects in monolayer *h*-BN for quantum bit and emitter applications. We choose *n*-type defects which are closely related to common intrinsic and extrinsic defects in BN and can potentially create several occupied defect levels in the band gap and high spin states. For each candidate defect, we examine the charge transition level (CTL) which determines the stability ranges of various charge states of each defect. For each stable charge state, we evaluate spin states and optical excitations along different polarization directions. With these calculations, we will show C_BV_N (a nitrogen vacancy adjacent to boron substituted by carbon, as shown in Fig. 1) to be the most promising defect in 2D *h*-BN, analogous to the NV center in 3D diamond, which has a stable triplet ground state and a bright anisotropic optical transition between defect levels.

However, calculating the properties such as CTLs and optical excitations of charged defects in 2D materials present serious challenges for state-of-the-art first-principles methods, which have so far limited the accuracy of previous calculations. We start this Rapid Communication by outlining these challenges and then discuss our methodology to address them.

The formation energy of a defect in charge state q, ionic coordinates $\mathbf{R}$, and electron chemical potential ε_F (often set to the valence band maximum for insulators or semiconductors) is given by [19]

$$E_q^f(\mathbf{R})[\varepsilon_F] = E_q(\mathbf{R}) - E_{\mathrm{pst}} + \sum_i \mu_i \Delta N_i + q\varepsilon_F. \quad (1)$$

Here, $E_q(\mathbf{R})$ is the total energy of the system with the charged defect, and E_{pst} is the total energy of the pristine system.

*yuanping@ucsc.edu

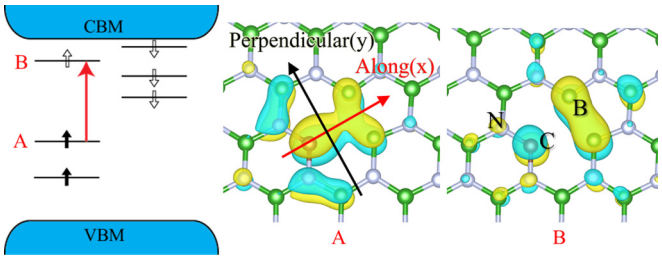

FIG. 1. Left: C_BV_N defect energy levels in monolayer BN with spin up (up arrow) and spin down (down arrow) channels, respectively. The black solid arrows represent occupied states and open arrows represent unoccupied states. The red arrow represents the bright transition between two defect states. Right: The wave functions for the two defect states ("A" and "B") that have the bright optical transition. "Perpendicular" and "Along" are two orthogonal directions in the plane; only the "Along" direction has the bright transition.

The third term on the right-hand side accounts for the change ΔN_i in the number of atoms of element i between these two configurations, with μ_i being the atomic chemical potential of that element in its stable form. The thermodynamic charge transition level (CTL) is the value of the electron chemical potential at which the stable charge state of the defect changes from q to $q+1$, which corresponds to equal formation energies of the q and $q+1$ states, and is therefore given by

$$\varepsilon^{q+1|q} = E_q^f(\mathbf{R}_q) - E_{q+1}^f(\mathbf{R}_{q+1}), \tag{2}$$

where $\mathbf{R}_q$ are the ionic coordinates of the charge state q. We note that the defect ionization energies associated with thermodynamic CTLs include the vertical excitation energy between two charge states and a geometry relaxation energy at the final charge state [19]. The vertical excitation energy is related to the optical CTLs, which can be directly obtained from quasiparticle band structures. In this Rapid Communication, we denote the thermodynamic charge transition level as "CTL," unless specified.

Within density functional theory (DFT), CTLs can be determined by calculating the formation energies in Eq. (2) in their respective equilibrium geometries, but this introduces two problems. First, DFT calculations of defects employ periodic boundary conditions on a supercell; the formation energies of charged defects converge very slowly with supercell sizes due to periodic charge interactions, and this is even more problematic for 2D materials. Second, the well-known band gap problem and self-interaction errors within standard DFT methods introduce significant errors in calculated CTLs, even if the supercell convergence issue could be dealt with.

The second issue above can be effectively solved by combining DFT with the many-body perturbation theory GW method [20–23]. This involves rewriting the CTL calculation as [23–25]

$$\varepsilon^{q+1|q} = \underbrace{E_q^f(\mathbf{R}_q) - E_{q+1}^f(\mathbf{R}_q)}_{E_{\rm QP}} + \underbrace{E_{q+1}^f(\mathbf{R}_q) - E_{q+1}^f(\mathbf{R}_{q+1})}_{E_{\rm rlx}}, \tag{3}$$

by adding and subtracting $E_{q+1}^f(\mathbf{R}_q)$ [we note that the results are insensitive to the choice of path for defects in monolayer BN, as discussed in the Supplemental Material (SM) [26]]. The second pair of terms on the right-hand side of Eq. (3) is the structural relaxation energy $E_{\rm rlx}$ at the charge state q, which can be calculated with reasonable accuracy at the DFT level (provided we solve the periodic charge interaction issue). The first pair of terms in Eq. (3) is the quasiparticle (QP) excitation energy $E_{\rm QP}$ at the fixed geometry $\mathbf{R}_q$, which can be calculated accurately using the GW method [20,27,28]. However, GW calculations of quasiparticle energies in 2D materials exhibit serious convergence difficulties [29–31] that make the calculations of charged defects that require large supercells extremely challenging.

At this stage, Eq. (3) provides accurate CTLs in principle, provided we can address the periodic charge interaction issue in the formation energies of charged defects at the DFT level, and resolve convergence issues for GW calculations of 2D materials. Below, we discuss each of these two issues and our methodology to overcome them.

First, the basic problem in charged defect formation energy calculations in DFT is the spurious interaction of the charged defect with its periodic images and with the uniform compensating background charge (necessary to make the total energy finite). For 3D systems, correction schemes [32–35] by removing the spurious periodic interaction from the DFT results using a model charge distribution for the defect and a model dielectric response for the bulk material work reliably well, because the self-energies of a model charge distribution both with periodic boundary conditions and without, i.e., the isolated case can be computed easily [32].

However, for 2D materials, the dielectric screening is strongly anisotropic and localized to one atomic layer; correction schemes now require a spatially dependent anisotropic dielectric function, whose spatial profile is not unambiguously defined. Most importantly, the calculation of the isolated charge self-energy for the correction has so far relied on extrapolating periodic calculations in various supercell sizes [36], an approach we find here to be problematic due to its strong nonlinear dependence on the supercell sizes [as shown in Fig. 2(a)]. This nonlinearity comes from both the highly anisotropic screening in monolayer 2D materials and the spatial distribution of the bound charge in the dielectric surrounding the model charge, which is even more important for the charged defects of MoS_2 [37], which has a larger in-plane dielectric constant than h-BN.

We recently developed a robust scheme for calculating the formation energies of charged defects in bulk and interfaces [38], that (a) redefines DFT electrostatic potentials to avoid strong oscillations near the atom centers, improving supercell convergence with geometry optimization, (b) unambiguously defines a spatial dielectric profile $\epsilon^{-1}(z) = \frac{-\partial \Delta V(z)}{E_0 \partial z}$ as the change in the now-smooth total potential $\Delta V(z)$ upon applying a normal electric field E_0, and, importantly, (c) it also completely avoids the problematic extrapolation between supercell sizes [36] (or convergence issues in image charge methods [33]) by using a spectral expansion in cylindrical Bessel functions for the isolated electrostatic energy. Here, we extend all aspects of that approach to handle the anisotropic dielectric response in 2D materials (see SM [26]), including an exact calculation of the isolated electrostatic self-energy. Figure 2(a) shows that the conventional extrapolation techniques line up to

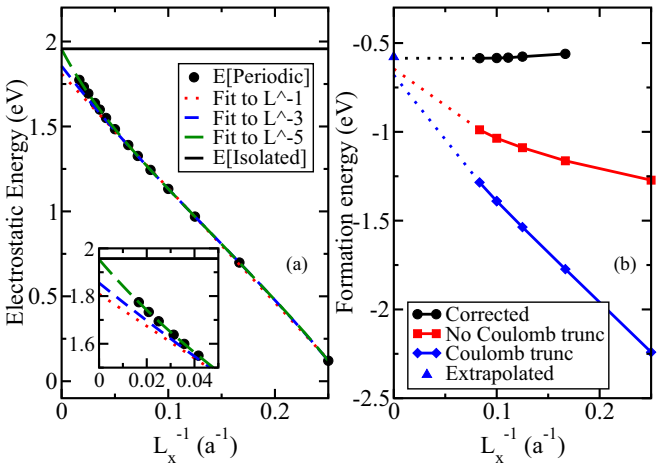

FIG. 2. Electrostatic self-energies of a model charge in a 2D slab with the periodic boundary condition (black dots) and the isolated boundary condition (black line). Dashed red, blue, and green lines are fitting curves to the periodic electrostatic self-energies with a different order of polynomials. (b) Formation energies of C_B (+1) defect at different supercell sizes L (where $a = 2.50$ Å is the lattice constant of h-BN). With conventional periodic Coulomb interactions (red squares), the cell size scales with $L_z = L_x$, while with truncated Coulomb potentials (blue diamonds), L_z is constant with a 15-bohr vacuum. With our correction scheme (black dots), results are converged to within 10 meV in a 6×6 a^2 cell. The extrapolated result (blue triangle) includes a correction based on the fitted results from (a).

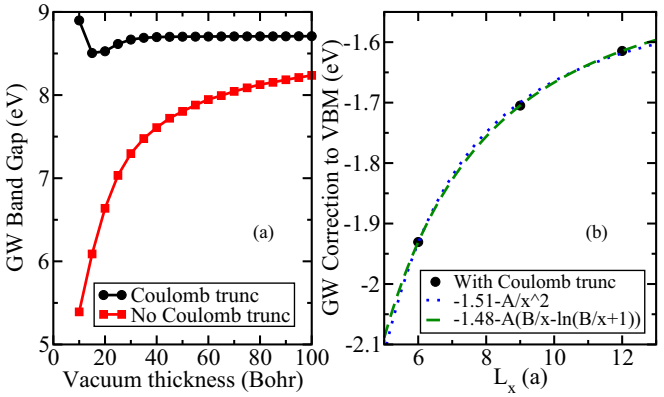

FIG. 3. (a) Coulomb truncation substantially improves convergence of the GW band gap of h-BN with respect to vacuum spacing (with a 3×3 a^2 lateral supercell size). (b) GW correction to the valence band maximum (VBM) extrapolates reliably with a lateral supercell size. The black dots are the computed values with Coulomb truncation and the dotted blue and dashed green lines are extrapolated values with two different formulas.

this result, but only when those fits are done to a high enough order (e.g., fifth order).

Figure 2(b) shows that our charge correction scheme (black dots) converges the C_B (+1) charged defect formation energy within 10 meV in a 6×6 supercell, with a converged value of -0.59 eV. The formation energy without the correction and with an isotropic supercell extrapolation by a third-order polynomial (red line) gives a similar result with Ref. [36], but fails to account for the nonlinearity of the periodic model charge self-energy with the supercell sizes. The difference between our method (black dots) and this extrapolated result (red line) in Fig. 2(b) is 0.12 eV, which lines up exactly with the difference between third- and fifth-order extrapolations in Fig. 2(a). We therefore expect that previous predictions of the charged defect formation energies in 2D materials could routinely contain inaccuracies of this magnitude, or even larger for 2D materials with a higher in-plane dielectric constant.

The second major issue is the extremely slow numerical convergence of the GW method for 2D materials, in part because of the rapid spatial variation in screening along the vacuum direction [29,39]. These issues have produced large discrepancies in the literature even for the properties of pristine 2D materials [29,31]. As an example, converging GW calculations of pristine monolayer MoS_2 require at least 6000 bands, 25 Å vacuum spacing, and a $24 \times 24 \times 1$ k-point grid for Brillouin zone integration [29]. Adopting such parameters for large supercell calculations containing defects would make them impractical.

The slow convergence with respect to the number of bands can be overcome by using a recent implementation of the GW method that does not explicitly require any empty states as implemented in the WEST code [20,21,28,40–42], based on density functional perturbation theory [43] and the projective dielectric eigenpotential (PDEP) algorithm [44,45].

For 2D materials, the remaining convergence issues arise from the long-range nature of the dielectric matrix and GW self-energy (in contrast to DFT), which have not been solved by current implementations. Here, the polarization of repeated images in the direction perpendicular to the plane spuriously screens the Coulomb interaction and lowers the QP gap [29]. These image interactions can be avoided in the correlation part of the self-energies by using a truncated Coulomb potential,

$$\bar{v}(\mathbf{k}) = \frac{4\pi}{k^2}\left(1 - e^{-k_{xy}L_z/2}\cos\frac{k_z L_z}{2}\right), \tag{4}$$

expressed here in reciprocal space [46]. In Eq. (4) we have $\mathbf{k} = \mathbf{q} + \mathbf{G}$, where $\mathbf{q}$ is a wave vector in the first Brillouin zone and $\mathbf{G}$ denotes the reciprocal lattice vectors. Figure 3(a) shows that this truncation results in excellent convergence with vacuum spacing for the GW QP gap of monolayer BN [specifically, we performed G_0W_0 calculations in which the self-energy is approximated from DFT states with the Perdew-Burke-Ernzerhof (PBE) exchange-correlation functional [47]]. At 30 bohrs (16 Å), the QP gap is converged within 10 meV, while the conventional treatment results in a smaller gap, as discussed above, which does not converge even at 100 bohrs.

When $\mathbf{G} = \mathbf{0}$ and $q_z = 0$, the potential in Eq. (4) diverges as $2\pi L_z/q_{xy}$ for $q_{xy} \to 0$ and the inverse dielectric matrix has a "dip" feature in this limit [29]. Accordingly, around the Γ point, a fine q mesh is required to compute absolute QP energies [31]. Explicit q-mesh convergence is not practical for large supercell calculations with defects. Instead, since discarding the $q_{xy} = 0$ component introduces an error proportional to L^{-2}, we extrapolate quasiparticle corrections to the $L \to \infty$ limit from three supercell sizes ($L^2 = 6 \times 6$, 9×9, 12×12 a^2). Figure 3(b) shows that this extrapolation works very well, with a deviation within 0.03 eV with respect to more

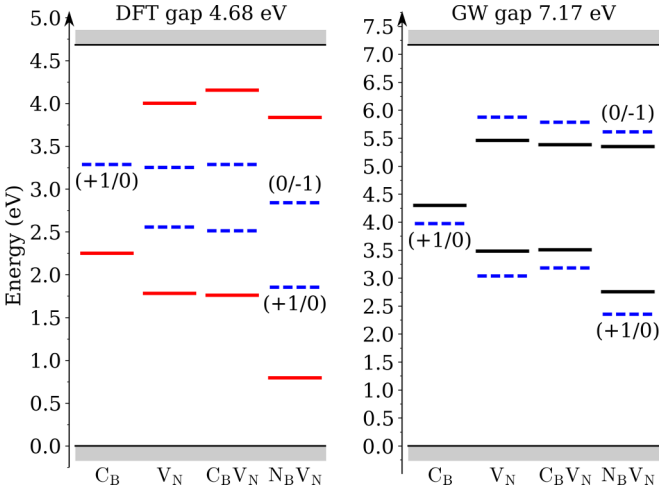

FIG. 4. Charge transition levels of various defects in h-BN computed by DFT (left panel) and GW (right panel) methods. Solid lines indicate the thermodynamic charge transition levels [Eq. (1) for DFT, Eq. (3) for GW], while dashed lines indicate the optical charge transition levels. We note that the optical CTLs are obtained from the eigenvalues at the DFT and GW levels of theory, respectively, at a fixed geometry. The Fermi level ε_F is set to the VBM of pristine h-BN. All defects have $(+1/0)$ and $(0/-1)$ CTLs inside the band gap, except C_B, which only has $(+1/0)$.

sophisticated models for the $\mathbf{q} \to \mathbf{0}$ contribution [31] (see Ref. [48]). The QP correction for the 12×12 a^2 is converged within 0.1 eV compared to the extrapolated value.

We implemented the DFT charge correction scheme discussed above in JDFTX [49] and the method to treat 2D materials in GW calculations in WEST [42]. Optimized geometry and DFT eigenvalues and wave functions are obtained using QUANTUM ESPRESSO [50]. (See SM [26] for further computational details.)

Having eliminated all the roadblocks in calculating the CTLs of 2D materials, we now predict the properties of the simple [C_B (carbon substitution of boron), V_N (nitrogen vacancy)] and complex [C_BV_N, N_BV_N (nitrogen substitution of boron adjacent to a nitrogen vacancy)] charged defects (C_BV_N; see Fig. 1). As discussed earlier, promising candidate defects should have stable high-spin states, localized and deep defect levels, spin-conserved excitations, and an anisotropic optical response [10,13]. Figure 4 shows their optical (without geometry relaxation at the final charge state, dashed lines) and thermodynamic CTLs (solid lines) at both the DFT (left panel) and GW (right panel) levels of theory (see Ref. [51]).

Figure 4 directly leads to several important conclusions. At both the DFT and GW levels of theory, all four types of defects have deep CTLs and localized defect wave functions (not shown). We note that we also performed hybrid functional calculations for the defective system, which partially correct the self-interaction errors in DFT, and found the defect geometry, ground spin state, and defect wave functions are similar between hybrid and semilocal functionals (see SM [26] for more details). The difference of thermodynamic CTL by DFT+GW in Eq. (3) and optical CTL by GW QP energies, which is the geometric relaxation energy, is less than 0.5 eV. The large difference between thermodynamic and optical CTLs in DFT is consistent with the fact that the total energies in DFT are more reliable than the eigenvalues, as the optical CTLs are directly computed from the eigenvalues, which do not have a strict physical meaning in DFT and cannot be interpreted as quasiparticle excitation energies. In fact, correcting the VBM (and CBM) reference in the DFT thermodynamic CTLs [using Eq. (1)] with GW QP energies yields a 0.1 eV difference compared to the full DFT+GW calculations of the CTLs [using Eq. (3)].

TABLE I. Physical properties of defects in monolayer h-BN relevant for quantum technologies. Below, "S," "D," and "T" denote singlet, doublet, and triplet spin states, respectively.

Defects	C_B	V_N	N_BV_N	C_BV_N
Deep level	Yes	Yes	Yes	Yes
Spin at $q = 0$	D	D	D	T
Spin at $q = \pm 1$	S	S	S	D
Bright transition between defect states	No	No	Yes	Yes
Optical anisotropy	No	No	Yes	Yes

All four defects have deep CTLs with the neutral state being stable for a wide range of ε_F, but their spin and optical properties are rather different, as Table I shows. The C_BV_N center has a spin triplet ground state, as shown in the left panel of Fig. 1, which is advantageous for quantum applications [10], distinct from the doublet state in other defects. Furthermore, we computed the optical transitions and absorption spectra for all defect cases and found both C_BV_N and N_BV_N have bright defect-to-defect state transitions well separated by over 1 eV from any defect-bulk and bulk-bulk transitions. A strong in-plane polarization anisotropy was also found in their absorption spectra (see Fig. 1 and SM [26] for details of the absorption spectra and selection rules).

In summary, we developed a methodology to reliably calculate thermodynamic CTLs in 2D materials by solving several critical issues in charged defect formation energies and GW QP energies for 2D systems in general. The source of difficulties originates from the highly anisotropic and localized screening of 2D systems, which necessitates a proper treatment of the electrostatic potentials of charges near a 2D plane and of the screened Coulomb interaction in the GW approximation. Using this methodology, we examined several possible defects in h-BN and identified the C_BV_N center to be promising for quantum technologies, which has multiple deep defect levels, a triplet ground state, and bright defect-to-defect transitions.

We thank Hosung Seo, Marco Govoni, Giulia Galli, and Jairo Velasco for many useful discussions. This research is supported by the startup funding of the Department of Chemistry and Biochemistry at the University of California, Santa Cruz, as well as the Department of Materials Science and Engineering at Rensselaer Polytechnic Institute. D.R. acknowledges financial support from Agence Nationale de la Recherche (France) under Grant No. ANR-15-CE29-0003-01. This research used resources of the Center for Functional Nanomaterials, which is a US DOE Office of Science Facility, at Brookhaven National Laboratory under Contract No. DE-SC0012704, the National Energy Research Scientific Comput-

ing Center (NERSC), a DOE Office of Science User Facility supported by the Office of Science of the US Department of Energy under Contract No. DEAC02-05CH11231, and the Extreme Science and Engineering Discovery Environment (XSEDE), which is supported by National Science Foundation Grant No. ACI-1548562 [52].

[1] S. Z. Butler, S. M. Hollen, L. Cao, Y. Cui, J. A. Gupta, H. R. Gutiérrez, T. F. Heinz, S. S. Hong, J. Huang, A. F. Ismach, E. Johnston-Halperin, M. Kuno, V. V. Plashnitsa, R. D. Robinson, R. S. Ruoff, S. Salahuddin, J. Shan, L. Shi, M. G. Spencer, M. Terrones, W. Windl, and J. E. Goldberger, ACS Nano **7**, 2898 (2013).

[2] A. Splendiani, L. Sun, Y. Zhang, T. Li, J. Kim, C.-Y. Chim, G. Galli, and F. Wang, Nano Lett. **10**, 1271 (2010).

[3] K. S. Novoselov, V. I. Fal'ko, L. Colombo, P. R. Gellert, M. G. Schwab, and K. Kim, Nature (London) **490**, 192 (2012).

[4] A. Pakdel, Y. Bando, and D. Golberg, Chem. Soc. Rev. **43**, 934 (2014).

[5] Z. Wu and Z. Ni, Nanophotonics **6**, 1219 (2017).

[6] T. T. Tran, C. Elbadawi, D. Totonjian, C. J. Lobo, G. Grosso, H. Moon, D. R. Englund, M. J. Ford, I. Aharonovich, and M. Toth, ACS Nano **10**, 7331 (2016).

[7] I. Aharonovich and M. Toth, Science **358**, 170 (2017).

[8] D. Wong, J. Velasco, Jr., L. Ju, J. Lee, S. Kahn, H.-Z. Tsai, C. Germany, T. Taniguchi, K. Watanabe, A. Zettl, F. Wang, and M. F. Crommie, Nat. Nanotechnol. **10**, 949 (2015).

[9] J. Velasco, L. Ju, D. Wong, S. Kahn, J. Lee, H.-Z. Tsai, C. Germany, S. Wickenburg, J. Lu, T. Taniguchi, K. Watanabe, A. Zettl, F. Wang, and M. F. Crommie, Nano Lett. **16**, 1620 (2016).

[10] J. R. Weber, W. F. Koehl, J. B. Varley, A. Janotti, B. B. Buckley, C. G. Van de Walle, and D. D. Awschalom, Proc. Natl. Acad. Sci. USA **107**, 8513 (2010).

[11] W. F. Koehl, H. Seo, G. Galli, and D. D. Awschalom, MRS Bull. **40**, 1146 (2015).

[12] H. Seo, M. Govoni, and G. Galli, Sci. Rep. **6**, 20803 (2016).

[13] F. Jelezko, T. Gaebel, I. Popa, M. Domhan, A. Gruber, and J. Wrachtrup, Phys. Rev. Lett. **93**, 130501 (2004).

[14] T. T. Tran, K. Bray, M. J. Ford, M. Toth, and I. Aharonovich, Nat. Nanotechnol. **11**, 37 (2016).

[15] Z. Shotan, H. Jayakumar, C. R. Considine, M. Mackoit, H. Fedder, J. Wrachtrup, A. Alkauskas, M. W. Doherty, V. M. Menon, and C. A. Meriles, ACS Photonics **3**, 2490 (2016).

[16] A. L. Exarhos, D. A. Hopper, R. R. Grote, A. Alkauskas, and L. C. Bassett, ACS Nano **11**, 3328 (2017).

[17] S. Choi, T. T. Tran, C. Elbadawi, C. Lobo, X. Wang, S. Juodkazis, G. Seniutinas, M. Toth, and I. Aharonovich, ACS Appl. Mater. Interfaces **8**, 29642 (2016).

[18] S. A. Tawfik, S. Ali, M. Fronzi, M. Kianinia, T. T. Tran, C. Stampfl, I. Aharonovich, M. Toth, and M. J. Ford, Nanoscale **9**, 13575 (2017).

[19] C. Freysoldt, B. Grabowski, T. Hickel, J. Neugebauer, G. Kresse, A. Janotti, and C. G. Van de Walle, Rev. Mod. Phys. **86**, 253 (2014).

[20] M. Govoni and G. Galli, J. Chem. Theory Comput. **11**, 2680 (2015).

[21] Y. Ping, D. Rocca, and G. Galli, Chem. Soc. Rev. **42**, 2437 (2013).

[22] M. Jain, J. R. Chelikowsky, and S. G. Louie, Phys. Rev. Lett. **107**, 216803 (2011).

[23] P. Rinke, A. Janotti, M. Scheffler, and C. G. Van de Walle, Phys. Rev. Lett. **102**, 026402 (2009).

[24] A. Malashevich, M. Jain, and S. G. Louie, Phys. Rev. B **89**, 075205 (2014).

[25] W. Chen and A. Pasquarello, J. Phys.: Condens. Matter **27**, 133202 (2015).

[26] See Supplemental Material at http://link.aps.org/supplemental/10.1103/PhysRevMaterials.1.071001 for computational details, sensitivity of model parameters in charge correction, convergence of GW calculations, bandstructures and absorption spectra of defects in h-BN.

[27] W. Chen and A. Pasquarello, Phys. Rev. B **96**, 020101 (2017).

[28] T. A. Pham, H.-V. Nguyen, D. Rocca, and G. Galli, Phys. Rev. B **87**, 155148 (2013).

[29] D. Y. Qiu, F. H. da Jornada, and S. G. Louie, Phys. Rev. B **93**, 235435 (2016).

[30] F. Hüser, T. Olsen, and K. S. Thygesen, Phys. Rev. B **87**, 235132 (2013).

[31] F. A. Rasmussen, P. S. Schmidt, K. T. Winther, and K. S. Thygesen, Phys. Rev. B **94**, 155406 (2016).

[32] C. Freysoldt, J. Neugebauer, and C. G. Van de Walle, Phys. Rev. Lett. **102**, 016402 (2009).

[33] H. P. Komsa, T. Rantala, and A. Pasquarello, Physica B **407**, 3063 (2012).

[34] Y. Kumagai and F. Oba, Phys. Rev. B **89**, 195205 (2014).

[35] D. Wang, D. Han, X. B. Li, S. Y. Xie, N. K. Chen, W. Q. Tian, D. West, H. B. Sun, and S. B. Zhang, Phys. Rev. Lett. **114**, 196801 (2015).

[36] H. P. Komsa, N. Berseneva, A. V. Krasheninnikov, and R. M. Nieminen, Phys. Rev. X **4**, 031044 (2014).

[37] J.-Y. Noh, H. Kim, and Y.-S. Kim, Phys. Rev. B **89**, 205417 (2014).

[38] R. Sundararaman and Y. Ping, J. Chem. Phys. **146**, 104109 (2017).

[39] C. Attaccalite, M. Bockstedte, A. Marini, A. Rubio, and L. Wirtz, Phys. Rev. B **83**, 144115 (2011).

[40] H.-V. Nguyen, T. A. Pham, D. Rocca, and G. Galli, Phys. Rev. B **85**, 081101 (2012).

[41] D. Rocca, J. Chem. Phys. **140**, 18A501 (2014).

[42] http://www.west-code.org, downloaded 2017-6-1.

[43] S. Baroni, S. de Gironcoli, and A. Dal Corso, Rev. Mod. Phys. **73**, 515 (2001).

[44] H. F. Wilson, F. Gygi, and G. Galli, Phys. Rev. B **78**, 113303 (2008).

[45] H. F. Wilson, D. Lu, F. Gygi, and G. Galli, Phys. Rev. B **79**, 245106 (2009).

[46] S. Ismail-Beigi, Phys. Rev. B **73**, 233103 (2006).

[47] J. P. Perdew, K. Burke, and M. Ernzerhof, Phys. Rev. Lett. **77**, 3865 (1996).

[48] Refrence [31] shows that the $\mathbf{q} \to \mathbf{0}$ (and $\mathbf{G} = \mathbf{0}$) contribution to the self-energy is proportional to $\ln(1 + c/L) - c/L$ [Eq. (A31) therein], which reduces to L^{-2} at the leading order.

[49] R. Sundararaman, K. Letchworth-Weaver, K. A. Schwarz, D. Gunceler, Y. Ozhabes, and T. A. Arias, SoftwareX **6**, 278 (2017).

[50] P. Giannozzi, S. Baroni, N. Bonini, M. Calandra, R. Car, C. Cavazzoni, D. Ceresoli, G. L. Chiarotti, M. Cococcioni, I. Dabo, A. Dal Corso, S. de Gironcoli, S. Fabris, G. Fratesi, R. Gebauer, U. Gerstmann, C. Gougoussis, A. Kokalj, M. Lazzeri, L. Martin-Samos, N. Marzari, F. Mauri, R. Mazzarello, S. Paolini, A. Pasquarello, L. Paulatto, C. Sbraccia, S. Scandolo, G. Sclauzero, A. P. Seitsonen, A. Smogunov, P. Umari, and R. M. Wentzcovitch, J. Phys.: Condens. Matter **21**, 395502 (2009).

[51] We note that the discussion on the numerical issues and procedures to solve them is general and valid both for the self-consistent GW and one-shot G_0W_0 approach. Specifically, in this work, we performed G_0W_0 calculations starting from DFT electronic states generated with the PBE exchange-correlation functional.

[52] J. Towns, T. Cockerill, M. Dahan, I. Foster, K. Gaither, A. Grimshaw, V. Hazlewood, S. Lathrop, D. Lifka, G. D. Peterson, R. Roskies, J. R. Scott, and N. Wilkens-Diehr, Comput. Sci. Eng. **16**, 62 (2014).